Chinese Chemical Letters 34 (2023) 107969

Contents lists available at ScienceDirect

Chinese Chemical Letters

journal homepage: www.elsevier.com/locate/cclet

Dual-active-site Fe/Cu single-atom nanozymes with multifunctional specific peroxidase-like properties for S^{2-} detection and dye degradation

Xiaofang Chen[a], Ya Wang[a,*], Min Feng[a], Die Deng[a], Xiaoyi Xie[a], Caixia Deng[b], Kashif Nawaz Khattak[a], Xiupei Yang[a,*]

[a] College of Chemistry and Chemical Engineering, Chemical Synthesis and Pollution Control Key Laboratory of Sichuan Province, China West Normal University, Nanchong 637000, China
[b] College of Environmental Science and Engineering, China West Normal University, Nanchong 637000, China

ARTICLE INFO

Article history:
Received 31 August 2022
Revised 18 October 2022
Accepted 1 November 2022
Available online 4 November 2022

Keywords:
Single-atom nanozymes
Dual active sites
Peroxidase-like catalyst
Colorimetric detection
Dye degradation

ABSTRACT

Designing single-atom nanozymes with densely exposed metal atom active sites and enhancing catalytic activity to detect pollutants remain a serious challenge. Herein, we reported a single-atom nanozyme with layered stacked Fe/Cu dual active sites (Fe/Cu-NC SAzyme) synthesized *via* hydrothermal and high-temperature pyrolysis using folic acid as a template. Compared with Fe-NC and Cu-NC SAzyme, Fe/Cu-NC SAzyme has higher peroxidase-like activity, which indicates that the doping of synthesized Fe/Cu bimetals can improve the catalytic activity and that the atomic loading of Fe and Cu in Fe/Cu-NC is 5.5 wt% and 2.27 wt%, respectively. When S^{2-} is added to the Fe/Cu-NC catalytic system, a high-sensitivity and high-selectivity S^{2-} colorimetric sensing platform can be established, with a wide linear range (0.09–6 μmol/L) and a low detection limit (30 nmol/L), which can be used to detect S^{2-} in environmental water samples. What's more, the Fe/Cu-NC SAzyme can activate peroxymonosulfate (PMS) to degrade 99.9% of rhodamine B (RhB) within 10 min with a degradation kinetics of 0.5943 min^{-1}. This work details attractive applications in Fe/Cu-NC SAzyme colorimetric sensing and dye degradation.

Sulfide (S^{2-}) widely exists in natural water, cosmetics, and industrial wastewater of sulfur dyes in the tanneries and food processing industries [1,2]. Notably, once the sulfide ion is protonated, it becomes the more toxic hydrogen sulfide (H_2S), which is considered to be one of the endogenous gas emitters [3–5]. Low concentrations of H_2S smell like rotten eggs, but high concentrations of H_2S are tasteless [1], and long-term exposure to low levels of sulfide can cause chronic diseases of the human respiratory tract, blood, eyes and digestive system, and even death [6]. Studies have shown that abnormal levels of hydrogen sulfide in the blood are closely related to many diseases, such as Alzheimer's disease [7], Down's syndrome [8] and liver cirrhosis [9]. Therefore, it is crucial to develop a simple, rapid, and sensitive method and on-site detection platform for the detection of S^{2-}. To date, a variety of methods have been developed for the detection of sulfides, including fluorescence [10], voltammetry [11], absorption [12], and colorimetry [13]. Colorimetry has attracted much attention due to its simplicity of operation, low cost and optical properties [14].

Nanozymes are a class of nanomaterials with enzyme-like properties and are considered to be a class of materials with great potential to replace traditional natural enzymes [15]. Due to the advantages of simple synthesis, tunable catalytic activity, good stability, low cost, and easy purification, nanozymes have become a research hotspot in the field of catalysis in recent years and are also promising alternatives to natural enzymes in various applications [16,17]. Although great progress has been made, the development of nanozymes is still hindered by several challenges.

In recent years, single-atom nanozymes with dispersed metal active sites have become substitutes for natural enzymes due to their advantages of 100% metal atom utilization [18], high activity [19], good selectivity [20] and low cost [21,22]. The M-N-C single-atom nanozyme has a similar M-N_x active site to the natural enzyme, which can more realistically mimic the active center of the natural enzyme and is helpful to understand its catalytic mechanism [23,24]. Theoretically, research on nanozymes accurately determined by the coordination structure is particularly important for revealing the source of their ability to mimic en-

* Corresponding authors.
E-mail addresses: ywang312@163.com (Y. Wang), xiupeiyang@cwnu.edu.cn (X. Yang).

https://doi.org/10.1016/j.cclet.2022.107969
1001-8417/

zymes [25], which is beneficial to promote the exploration of the catalytic mechanism and bridge the gap between nanozymes [26]. Our group designed and realized for the first time the controllable synthesis of b-doped Zn-N-C (ZnBNC) single-atom nanozymes (SAzymes) as efficient peroxidase mimics [14]. We also successfully synthesized Fe single-atom catalysts on fluorine-doped (Fe-SAs@FNC) ultrathin carbon nanosheets by polymer-assisted heating [22]. This lays a good foundation for our work.

To take full advantage of the efficient catalytic activity of SAzymes, we expect that it can be used not only for the sensing and detection of environmental pollutants, but also for the degradation of organic pollutants such as dyes. It is well known that the hydroxyl radicals generated in the Fenton-like reaction can easily degrade dyes, but there are still some limitations on dye degradation in the Fenton-like system, such as the narrow optimal pH value (pH 2–4) [27], the huge amount of iron hydroxide sludge [28], and the difficulty of catalyst recovery [29]. It greatly limits the practical application of Fenton-like systems for dye degradation. Therefore, if the highly dispersed metal sites, 100% atomic utilization, special electronic structure, good pH stability and excellent catalytic performance of SAzymes are utilized in the dye degradation process, it is expected to overcome the above-mentioned shortcomings in the dye degradation process.

Herein, a single-atom nanozyme (Fe/Cu-NC SAzyme) with bimetallic active sites was designed and synthesized by a one-pot hydrothermal method and pyrolysis method, which can be used for colorimetric detection of S^{2-} and degradation of dyes. When S^{2-} was added to the Fe/Cu-NC/TMB/H_2O_2 system, blue oxTMB was reduced to colorless TMB, thus constructing a colorimetric sensing platform for the detection of sulfide ions. A linear activity range of 0.09–6 μmol/L was obtained with a low detection limit of 30 nmol/L, which is superior to the most published optical S^{2-} assays. Fe/Cu-NC can also activate PMS to generate $SO_4^{\bullet-}$ and other free radicals and effectively degrade rhodamine B (RhB), malachite green oxalate (MG), and methylene blue (MB) within 10 min (Scheme 1). Therefore, the bifunctional role of Fe/Cu-NC SACs in detection and dye degradation was developed.

For material synthesis, folic acid powder (FA 550 mg), $FeCl_2{\cdot}4H_2O$ (0.125 g), and $CuCl_2{\cdot}2H_2O$ (0.1 g) were first dissolved in a mixture of 27.5 mL of ultrapure water and 40 mL of ethanol and stirred for 10 min. The mixture was hydrothermally treated at 140 °C for 2 h [30]. After the solution was cooled to room temperature, the brown precipitate was centrifuged, washed thoroughly with deionized water and freeze dried for use. For comparison, FA-Fe, FA-Cu and FA nanosheets were synthesized under the same conditions but in the absence of $FeCl_2{\cdot}4H_2O$, $CuCl_2{\cdot}2H_2O$ and metal salts, respectively. Then, the as-synthesized powders of FA-M were transferred into a ceramic boat and heated from room temperature to 700 °C at a heating rate of 5 °C/min under a N_2 atmosphere and then held at 700 °C for 2 h. Then, the obtained materials were naturally cooled to yield Fe/Cu-NC, Fe-NC, Cu-NC and NC samples. The details for various characterization of the above materials are provided in the Supporting information.

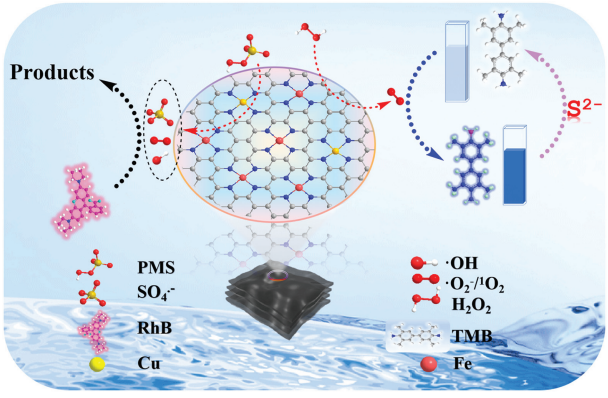

Scheme 1. Structural diagram of Fe/Cu-NC SAzymes and their application to the determination of S^{2-} and the degradation of dyes.

TMB was employed as a colorimetric substrate to verify the peroxidase-like features of Fe/Cu-NC. Typically, 10 μL of 2 mg/mL Fe/Cu-NC SAzymes was first added to 3 mL of pH 4.5 acetate buffer solution (HAc-NaAc buffer solution), and then 70 μL of 7.5 mmol/L TMB solution and 15 μL of 250 mmol/L hydrogen peroxide solution (H_2O_2) were added. After incubation at 20 °C for 27 min, the absorbance at 652 nm was measured by UV–vis spectroscopy. To understand the active substances that play a role in the reaction system, we carried out active radical trapping experiments. Isopropanol (IPA), ethylenediaminetetraacetic acid disodium salt (EDTA-2Na), and *p*-benzoquinone (PBQ) were used to capture hydroxyl radicals (•OH), electrons (e^-), and superoxide radicals ($^{\bullet}O_2^-$). The typical reaction was as follows: 10 μL of Fe/Cu-NC SAzymes, 70 μL TMB and 15 μL H_2O_2 were added to 3 mL of HAc-NaAc buffer solution, followed by the addition of different concentrations of scavenger, and the absorbance at 652 nm was recorded.

To detect the standard curve of sulfide ions, aqueous solutions of different concentrations of sodium sulfide, including buffer solutions, were added to 3 mL of the system, Fe/Cu-NC (10 μL 2 mg/mL), TMB (70 μL 7.5 mmol/L) and H_2O_2 (15 μL 250 mmol/L). After 27 min of incubation at room temperature, the absorption spectrum of the reaction solution was recorded at 652 nm. In addition, to demonstrate the selectivity of the method, the same operation was used to replace the sulfide ions with 10-fold concentrations of other ions. To verify the feasibility of the method for detecting sulfide ions, actual samples were tested. Tap water, drinking water and lake water were obtained from the laboratory of West China Normal University and Yuxiu Lake and filtered with a 0.2 μm membrane to remove the large particulates in advance. Then, S^{2-} at different concentrations (0.6, 1, 4 μmol/L) was added to tap water, drinking water and lake water. Assessing colorimetric feasibility using standard additives. After incubation in a water bath at 25 °C for 3 min, the absorbance of the solution was recorded at 652 nm.

To investigate the activation of PMS by Fe/Cu-NC SAzymes for dye degradation, all degradation experiments were performed in shake flasks containing 40 mL RhB (10 mg/L, initial pH 4.5) at 25 °C. Typically, 2.4 mL of catalyst (2 mg/mL) and 200 μL of 30 mg/mL PMS were added to 40 mL of RhB, MB, and MG (10 mg/L, pH 4.5), respectively. At a preset time, a certain amount of suspension was withdrawn and filtered by syringe with a 0.22 μm mixed fiber film for absorbance measurement.

In this work, Fe/Cu-NC single-atom nanozymes were synthesized by a hydrothermal method, and the synthesis step is schematically illustrated in Fig. 1a. Folic acid, rich in oxygen- and nitrogen-functional groups, is a natural ligand that facilitates the molecular assembly and chelation of metals [31]. Wang *et al.* confirmed that in a mixed solution of water and ethanol, folic acid powder has a slight solubility, and the α-carboxyl group is partially dissociated and effectively chelated with metal ions (Fe or Cu), as depicted in Fig. S1 (Supporting information) [32]. The synchronous assembly of the complex and molecules formed a supramolecular combination, which promoted the formation of the Fe/Cu-NC precursor. Next, the Fe/Cu-NC SAzyme with dual active sites (Fe-N_4 and Cu-N_4) was obtained by directly Pyrolyzing a mixture of the Fe/Cu-M precursor at 700 °C for 2 h under a N_2 atmosphere.

The morphology of Fe/Cu-NCs was characterized by SEM and TEM (Figs. 1b and c), revealing a layered and stacked structure without metal aggregation. As shown in Fig. S2 (Supporting information), the morphology of NC, Fe-NC, and Cu-NC is character-

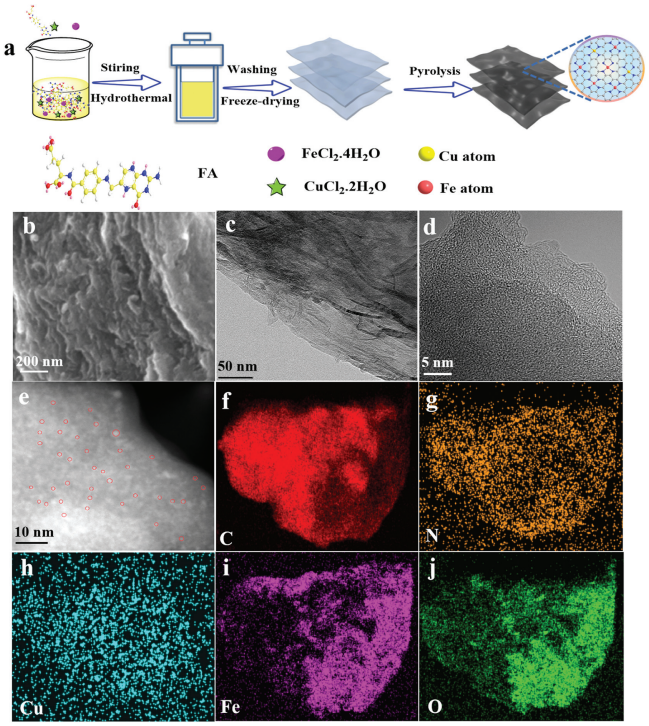

Fig. 1. (a) Schematic illustration of the synthesis of Fe/Cu-NC, (b) SEM, (c) TEM, (d) HRTEM, (e) HAADF-STEM images of Fe/Cu-NC, (f-j) corresponding EDS mapping images.

ized, and different degrees of flake structure are presented. HRTEM shows that there are no obvious crystals in Fe/Cu-NC, such as metal or metal composites, which indicates that Fe and Cu exist in the form of atoms (Fig. 1d). The high-angle annular dark-field-scanning transmission electron microscopy (HAADF-STEM) image shows numerous bright spots, indicating that atomically dispersed Fe and Cu sites are uniformly distributed on the carbon support (Fig. 1e) [33]. EDS elemental mapping confirmed that Fe, Cu, C, N, and O were uniformly distributed on the carbon framework (Figs. 1f-j and Fig. S3 in Supporting information) and that Fe and Cu were successfully doped into carbon-based nanosheets.

To further analyze the as-prepared Fe/Cu-NC SAzymes, we obtained X-ray (XRD) diffraction patterns and Raman spectra. It can be seen from Fig. S4a (Supporting information) that two broad peaks are displayed at 26° and 43°, which are the (002) and (101) crystal planes of carbon, respectively, and no diffraction peaks of active clusters of metal particles appear, which preliminarily proves that in this material, Fe and Cu exist in the form of atoms [34]. From the Raman spectra in Fig. S4b (Supporting information), it can be seen that the ratio of the D peak to the G peak increases from 1.3 to 3.0 after Fe-Cu codoping, which also proves that Fe-Cu codoping causes the carbon structure to increase the degree of defects and graphitization to decrease. In addition, there are no characteristic peaks of metal nanoparticles or clusters between 400 cm^{-1} and 700 cm^{-1} [35]. However, inductively coupled plasma-optical emission spectrometry (ICP-OES) determined an iron loading of 5.49 wt% and a copper loading of 2.27 wt%. The comprehensive analysis results show that iron and copper elements may be supported on the nanosheets in the form of atomic rather than crystalline or composite states.

The surface elemental composition and valence state of Fe/Cu-NC SAzymes were characterized by X-ray photoelectron spectroscopy (XPS). The XPS full spectrum of Fe/Cu-NC SAzymes shows the existence of Fe, Cu, N, C and O, indicating that Fe and Cu were successfully doped into the layered stacked nanosheets

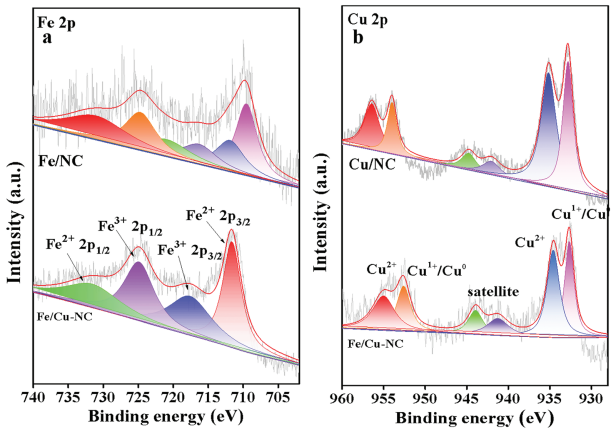

Fig. 2. High-resolution (a) Fe 2p and (b) Cu 2p spectra of Fe-NC, Cu-NC, and Fe/Cu-NC.

(Fig. S5 in Supporting information), which was consistent with the EDS results. The high-resolution N 1s spectrum has four peaks (Fig. S6a in Supporting information): pyridine-N (398.6 eV), M-N_x (400.15 eV), pyrrole-N (401.15 eV), and graphitic-N (403.50 eV) [36]. Among them, pyridine-N acts as an anchoring site for Fe and Cu atoms, and graphitic-N can affect the structure of carbon and improve the catalytic efficiency [37]. As depicted in Fig. S6b (Supporting information), the high-resolution O 1s spectrum of XPS has two characteristic peaks of C=O and C−O at 531.3 eV and 532.85 eV, respectively. Fig. S6c (Supporting information) shows that the C 1s spectrum is divided into four characteristic peaks, which correspond to C=C/C−C (284.8 eV), C−N/C−O (285.6 eV), C=N (288.45 eV), and C=O (291.6 eV) [38]. The Fe 2p spectrum displayed four peaks at 711.7 eV (Fe^{2+} $2p_{3/2}$), 717.75 eV (Fe^{3+} $2p_{3/2}$), 725.2 eV (Fe^{2+} $2p_{1/2}$), and 731.6 eV (Fe^{2+} $2p_{1/2}$) (Fig. 2a) [39,40] of which 711.7 eV represents the Fe-N_x active site [41]. As shown in Fig. 2b, the Cu 2p XPS spectrum presents two sets of peaks at binding energies of 932.7/952.8 eV and 934.5/955.0 eV that can be assigned to Cu^{1+}/Cu^0 and Cu^{2+} species, respectively, along with satellite peaks at 941–945 eV, which are characteristic of Cu^{2+} [5]. Hence, noncrystalline Cu-N_x species (Cu^{2+}, Cu^+) are present in Fe/Cu-NC, and the successful doping of Fe and Cu can be seen by XPS. According to previous reports and analyses of the structure, we speculate that the possible coordination environment of iron and copper is FeN_4 and CuN_4 [30,42]. This lays a good foundation for the improvement of enzyme activity.

To study the peroxidase-like activity of Fe/Cu-NC SAzymes, 3,3′,5,5′-tetramethylbenzidine (TMB) was used as the catalytic oxidation reaction substrate in the presence of H_2O_2. As depicted in Fig. 3a, Fe/Cu-NC/TMB/H_2O_2 exhibited high peroxidase-like activity at 652 nm (A_{652}). Conversely, the colors of individual substrates or substrate/H_2O_2 solutions change imperceptibly. To demonstrate the effect of bimetallic doping on the catalytic activity, the peroxidase-like activities of Fe/Cu-NC, Fe-NC, Cu-NC and NC were investigated. Fig. 3b shows that the NC/TMB/H_2O_2 system has no absorbance, indicating that the doping of metals can effectively improve the catalytic activity. Compared with Fe/Cu-NC/TMB/H_2O_2, the absorbance of the Fe-NC/TMB/H_2O_2 and Cu-NC/TMB/H_2O_2 reaction systems is weak, which proves that metal doping can improve the catalytic activity and that bimetallic active sites have higher catalytic activity than a single metal. As we expected, the introduction of Cu atoms significantly increased the peroxidase-like activity of the material, which would be beneficial to improving the sensitivity of colorimetric sensing. As a common transition metal element, Cu exists in various valence states (Cu^0, Cu^+, Cu^{2+}) [43] and has a rich electron transfer process, which has

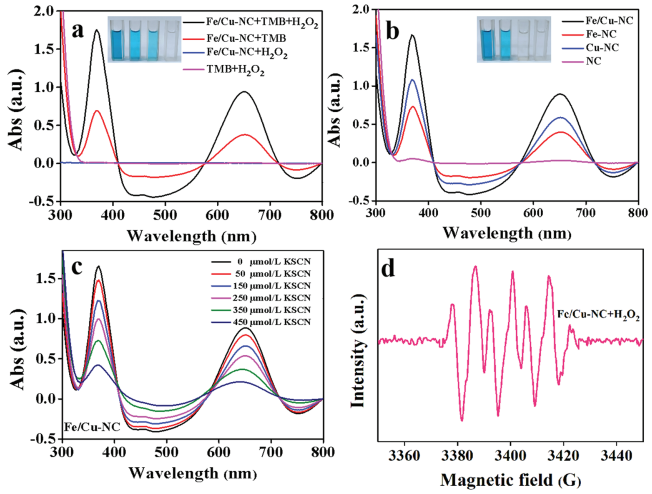

Fig. 3. (a) Study on peroxidase-like activity of Fe/Cu-NC single-atom catalysts. (b) Comparison of the UV–vis spectra of the enzyme-like activities of Fe-NC, Cu-NC, and Fe/Cu-NC (the inserted picture is a photo of the reaction under sunlight). (c) UV–vis spectra changes of Fe/Cu-NC/TMB/H_2O_2 solution upon the addition of various concentrations of SCN^-. (d) ESR spectra of the DMPO/$^{\bullet}O_2^-$ spin adduct of Fe/Cu-NC/H_2O_2.

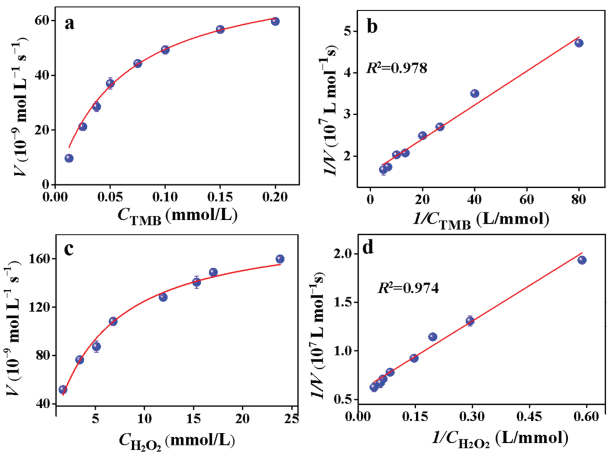

Fig. 4. Steady-state kinetic assay of the Fe/Cu-NC SAzymes for (a, b) TMB and (c, d) H_2O_2.

caused extensive research. Cu-based catalysts have high electrical conductivity and enhance the charge transfer between active sites and reactants, so copper doping may be a promising approach to construct nanozymes with high catalytic activity [44]. The partial combination of Fe and Cu can greatly improve the catalytic performance of single-atom nanozymes [45].

The catalytic ability of Fe/Cu-NC is affected by carbonization temperature, carbonization time, pH and reaction temperature (Figs. S7 and S8 in Supporting information). By comparison, we chose 700 °C as the pyrolysis time of Fe/Cu-NC (Fig. S7a). Gratifyingly, over a wide range of pyrolysis times (1–5 h), Fe/Cu-NC delivers good performance (Fig. S7b). It is worth noting that Fe/Cu-NC exhibited higher enzymatic activity at 20 °C and pH 4.5, which can be drawn from Figs. S8a and b. We also studied Fe/Cu-NCs, measuring A after treatment with 0.1 mol/L HCl and NaOH for different times, respectively. The experimental results show that the strong acid and strong alkali treatments have little effect on the catalytic activity of Fe/Cu-NC, indicating that Fe/Cu-NC has good acid and alkali resistance (Figs. S8c and d). To further study the stability of Fe/Cu-NC SAzymes, they were stored at room temperature, and the enzymatic activity was measured every 5 days. As shown in Fig. S9 (Supporting information), after 20 days, the enzymatic activity of Fe/Cu-NC SAzymes was reduced by only approximately 10%, indicating its high stability.

As we all know, SCN^-, as a strong chelating agent, can form stable complexes with catalytic sites of metals such as Fe, Cu and Co, thus breaking the active sites of metals [46,47]. As depicted in Fig. 3c, when Fe/Cu-NC (Fe-NC or Cu-NC) is added to the TMB/H_2O_2 system pretreated with KSCN at different concentrations, its catalytic activity is irreversibly inhibited by SCN^-, which indicates that Fe and Cu have a synergistic effect and have a greater contribution to the improvement of enzyme activity (Fig. S10 in Supporting information) [18]. It is impossible for NC to catalyze TMB oxidation without metal doping, and the doping of iron and copper can improve the catalytic activity, which proves that Fe-N_x sites or Cu-N_x sites play an indispensable role. However, the catalytic activity of a single metal is not greatly improved, and only when Fe and Cu are doped at the same time does it show excellent catalytic activity. The above results show that double catalytic sites and nitrogen doping can promote the catalytic activity of Fe/Cu-NC, which is necessary to improve the catalytic activity.

To further understand the catalytic mechanism, the intermediate reactive oxygen species (ROS, including $^{\bullet}OH$, e^- and $^{\bullet}O_2^-$) generated in the Fe/Cu-NC/TMB/H_2O_2 reaction system were investigated using radical scavengers such as IPA, EDTA, and PBQ. Fig. S11 (Supporting information) shows that in the Fe/Cu-NC/TMB/H_2O_2 system, the addition of IPA and EDTA-2Na leads to a slight change in A_{652}, while the addition of PBQ leads to a significant decrease in absorbance at 652 nm. The results show that superoxide radicals are the main active species in Fe/Cu-NC. The EPR test also further confirmed this experimental result (Fig. 3d) [48].

To evaluate the catalytic activity of Fe/Cu-NC SAzymes, the steady-state kinetics were investigated using TMB and H_2O_2 as substrates, and the steady-state kinetic constants were obtained. A typical Michaelis-Menten-Menten-like curve was obtained within the appropriate concentration range of TMB (Figs. 4a and b) and H_2O_2 (Figs. 4c and d). The Michaelis-Menten constants K_m of TMB and H_2O_2 are 0.05 and 5.07, respectively, which are lower than those of HRP and some single-atom nanozymes (Table S1 in Supporting information), which makes the substrate more accessible to the catalyst and may be beneficial for subsequent catalytic reactions. In addition, V_{max} is also higher than that of most reported catalysts. Meanwhile, from the highest K_w point of view, the Fe/Cu-NC single-atom nanozyme is also generally higher than the catalytic efficiency of other materials reported in the literature.

It has been reported that sulfide ions have the potential to inhibit the peroxidase performance of nanozymes, reduce the generation of oxTMB [49], and change the color of the system from blue to colorless. Based on the excellent catalytic performance of Fe/Cu-NC and the inhibitory effect of S^{2-} on the color reaction of TMB, it is reasonable to imagine the S^{2-} colorimetric activity assay (Fig. 5a). The feasibility of the proposed S^{2-} determination method was preliminarily evaluated (Figs. 5b and c). When S^{2-} is introduced into the sensing system, the color reaction and absorption spectrum will be reduced accordingly, the linear range of S^{2-} detection is 0.09–6 μmol/L, and the detection limit is 30 nmol/L, which is much lower than the level specified by the World Health Organization (15 μmol/L) [50]. Compared with other methods for detecting S^{2-} in Table S2 (Supporting information), this method has better potential applicability.

To evaluate the selectivity of Fe/Cu-NC to detect S^{2-}, the same method was used to add anions (Cl^-, CO_3^{2-}, HCO_3^-, SO_4^{2-}, F^-, AC^-, $H_2PO_4^-$, PO_4^{3-}, HPO_4^{2-}) and cations (Cu^{2+}, Ce^{3+}, Ca^{2+}, Ni^{2+}, Mg^{2+}, Mn^{2+}, Al^{3+}, Cr^{3+}, NH_4^+, K^+, Ag^+) as interference substances in the Fe/Cu-NC-TMB-H_2O_2 system, and the interference concentration was 10 times that of S^{2-} (Fig. S12 in Supporting information).

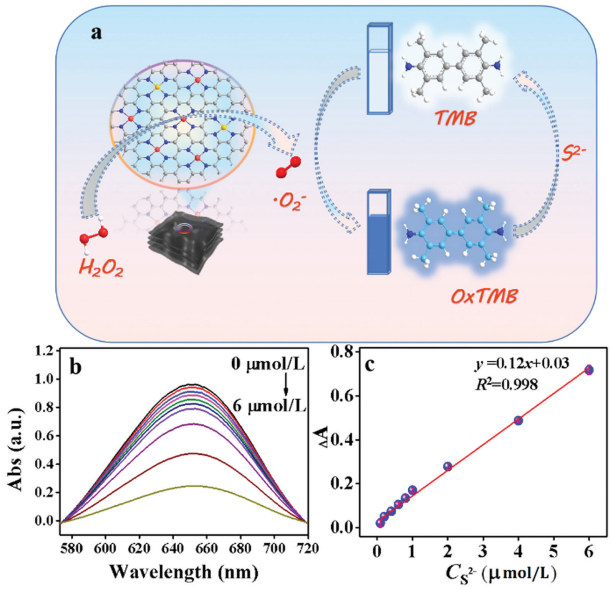

Fig. 5. (a) Schematic diagram of the colorimetric S^{2-} activity assay, (b) effects of different S^{2-} concentrations on the UV–vis spectra of Fe/Cu-NC SAzymes, (c) the linear relationship between the Abs and S^{2-} concentration. LOD = 30 nmol/L.

Table 1
Determination of S^{2-} in actual water samples.

Sample	Added (μmol/L)	Found (μmol/L)	Recovery (%)	RSD (%, $n = 3$)
Yuxiu lake	0.60	0.58 ± 0.02	96.67	3.45
	1.00	1.02 ± 0.04	101.7	3.92
	4.00	3.81 ± 0.06	95.18	1.57
Tap water	0.60	0.57 ± 0.01	95.41	1.75
	1.00	1.01 ± 0.01	100.6	0.99
	4.00	4.24 ± 0.03	106.1	0.71
Drinking water	0.60	0.63 ± 0.02	106.2	3.17
	1.00	1.05 ± 0.05	105.3	4.76
	4.00	3.97 ± 0.05	99.42	1.26

The excellent selectivity is profited from the guaranteed specificity of the enzymatic reaction and will facilitate the application of this method in the detection of S^{2-} in actual complex samples.

The method also evaluates the practical application value of sulfides in Yuxiu Lake, tap water, and drinking water. Table 1 shows that the recovery rate of the standard addition of the actual sample is between 95% and 106%, and the relative standard deviation (RSD) is calculated between 0.7% and 4.7%. Therefore, the proposed Fe/Cu-NC-based colorimetric detection S^{2-} platform has satisfactory sensitivity and practical application potential for the detection of actual samples.

Sulfate has a strong oxidizing ability and has a good degradation effect on some pollutants, for which it can be used in a wide pH range [51]. In particular, the activation of PMS by SAzymes can generate $SO_4^{\bullet-}$, $^{\bullet}O_2^-$ and other highly active species [52]. All the following degradation experiments were carried out under the optimal catalytic conditions and degradation conditions, among which there have been many reports exploring the optimal conditions for their degradation [53]. Therefore, their degradation properties were also investigated and applied to the refractory organic pollutant RhB. As shown in Fig. 6a, PMS itself has almost no ability to degrade RhB, while the Fe/Cu-NC single-atom catalyst has a slight degradation effect, and the degradation rate of RhB in the Fe/Cu-NC/PMS system can be reduced within 10 min to 100%.

Similarly, we explored the degradation effects of Fe/Cu-NC single-atom catalysts on MG and MB in the same way. As shown in Figs. S13a and b (Supporting information), the degradation effect of Fe/Cu-NC on MG and MB can also reach 100% within 10 min. To evaluate the catalytic performance and the degradation rates for different dyes, the reaction rate constants were investigated (k) calculated using a first-order kinetic model (inset in Fig. S13c in Supporting information. The k values for the degradation of RhB, MG, and MB were 0.5943 min^{-1}, 0.8218 min^{-1}, and 0.5702 $min^{-1,}$ respectively, which indicated the universality of degradation, and Fe/Cu-NC could also be used to degrade organic pollutants. Based on the better stability of the material, no iron-containing sludge is generated in the system, and the operation process is simpler, which shows that the proposed method has obvious advantages compared with the Fenton-like reaction to degrade dyes.

This study mainly takes RhB as an example to study the mechanism of the deorganization of organic dyes. Based on the scavenging effects of ethanol, L-his, TBA, and PBQ on $SO_4^{\bullet-}$, $^1O_2$, $^{\bullet}OH$, and $^{\bullet}O_2^-$ (Fig. 6b), quenching experiments with free radical scavengers were carried out to detect the main active substances in the degradation system [54,55]. The degradation rate of RhB decreased after the addition of ethanol, and k decreased from 0.6848 min^{-1} to 0.5119 min^{-1}, indicating the presence of $SO_4^{\bullet-}$ in the catalytic process (Fig. 6c). Moreover, ESR further confirmed the above conclusion. The characteristic peaks of $^{\bullet}O_2^-$ are observed in Fig. 6d, which is consistent with those reported in the literature [56]. As shown in Fig. 6e, a strong 1:1:1 tristate signal was observed soon after the addition of TEMP to the Fe/Cu-NC/PMS system, which further proved the existence of $^1O_2$ [50,57]. However, the Fe/Cu-NC/PMS/DMPO system shows characteristic signals for both DMPO-$SO_4^{\bullet-}$ and DMPO-$^{\bullet}OH$ adducts, which further demonstrates the coexistence of $^{\bullet}OH$ and $SO_4^{\bullet-}$ (Fig. 6f) [58]. The results showed that in addition to $SO_4^{\bullet-}$, $^{\bullet}OH$, $^1O_2$, and $^{\bullet}O_2^-$ also participated in the degradation process of RhB.

Based on the above results, $SO_4^{\bullet-}$, $^{\bullet}OH$, $^1O_2$ and $^{\bullet}O_2^-$ were generated during the degradation of RhB. Generally, the generation of $^{\bullet}OH$ and $SO_4^{\bullet-}$ may be the results of the electron transfer from M-N_4 to PMS in Fe/Cu-NC (Eqs. 1 and 2), while electron transport from PMS to the nitrogen-doped carbon network generates $SO_5^{\bullet-}$ in Fe/Cu-NC [51,59], which reacts with water molecules to generate $^1O_2$ (Eqs. 3 and 4), and N-doped carbon materials can activate PMS to generate $^{\bullet}O_2^-$ (Eq. 5) [60].

$$HSO_5^- + e^-(\text{from metal in Fe}/Cu-NC) \rightarrow SO_4^{\bullet-} + OH^- \quad (1)$$

$$SO_4^{\bullet-} + H_2O \rightarrow SO_4^{2-} + {}^{\bullet}OH + H^+ \quad (2)$$

$$HSO_5^- - e^-(\text{from metal in Fe/Cu-NC}) \rightarrow SO_5^{\bullet-} + H^+ \quad (3)$$

$$SO_5^{\bullet-} + H_2O \rightarrow {}^1O_2 + SO_4^{\bullet-} + 2H^+ \quad (4)$$

$$O_2 + e^- \rightarrow {}^{\bullet}O_2^- \quad (5)$$

By surveying the literature, we conjecture that the more efficient activation of PMS by Fe/Cu-NC is mainly due to the synergistic effect of dual catalytic sites (Fe-N_4 and Cu-N_4) [55].

In summary, we successfully prepared single-atom catalysts with Fe and Cu bimetallic active sites, which not only increased the loading of metal atoms but also increased the degree of defects, thereby improving the catalytic activity of the enzyme-like catalyst. Based on the excellent peroxidase-like activity of Fe/Cu-NC SACs, a highly selective and highly sensitive colorimetric detection platform for S^{2-} was established. Due to the ability of Fe/Cu-NC SACs to activate PMS, they were also applied to the degradation of organic dyes, and a 100% degradation efficiency could be achieved within 10 min. This provides an alternative detection method for the detection of S^{2-} in the environment and the risk assessment of the human hazard from the degradation of organic dyes.

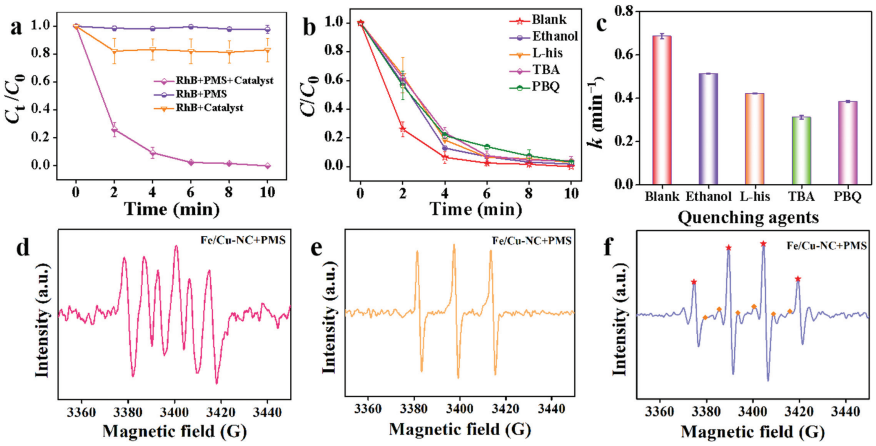

Fig. 6. (a) RhB degradation in different reaction systems, (b) degradation rates of different quenchers in the Fe/Cu-NC/PMS system, and (c) effects of different quenching agents on reaction rate constants in the Fe/Cu-NC/PMS system. (d) DMPO-trapped EPR spectra of $^{\bullet}O_2^-$. (e) TEMP-trapped EPR spectra of $^1O_2$. (f) DMPO-trapped EPR spectra of $SO_4^{\bullet-}$ and $^{\bullet}OH$ (★ represents DMPO-$^{\bullet}OH$, and ♦ represents DMPO-$SO_4^{\bullet-}$.

Declaration of competing interest

The authors declare that they have no known competing financial interests or personal relationships that could have appeared to influence the work reported in this paper.

Acknowledgments

This work is supported by the National Natural Science Foundation of China (Nos. 22276150, 21906129), the Natural Science Foundation of Sichuan Province of China (No. 2019YJ0522), and the Innovation Team of Research at China West Normal University (No. KCXTD2022–2).

Supplementary materials

Supplementary material associated with this article can be found, in the online version, at doi:10.1016/j.cclet.2022.107969.

References

[1] Y. Li, Y. Fang, W. Gao, et al., ACS Sustain. Chem. Eng. 8 (2020) 10870–10880.
[2] X. Liu, L. Huang, Y. Wang, et al., Sens. Actuators B: Chem. 306 (2020) 127565.
[3] Y. Jia, S. Wang, W. Chen, et al., Nanoscale 1 (2013) 1–3.
[4] H.Y. Li, S.N. Zhao, S.Q. Zang, et al., Chem. Soc. Rev. 49 (2020) 6364–6401.
[5] Y. Zhang, J. Zhao, H. Wang, et al., Nat. Commun. 13 (2022) 2062.
[6] K. Shanmugaraj, M. Ilanchelian, Microchim. Acta 183 (2016) 1721–1728.
[7] S. Bradburn, C. Murgatroyd, N. Ray, Ageing. Res. Rev. 50 (2019) 1–8.
[8] T. Panagaki, L. Lozano-Montes, L. Janickova, et al., Redox. Biol. 51 (2022) 102233.
[9] S. Fiorucci, E. Antonelli, A. Mencarelli, et al., Hepatology 42 (2005) 539–548.
[10] G. Zhang, R. Wang, L. Shi, et al., Sens. Actuators B: Chem. 279 (2019) 361–368.
[11] X. Cao, S. Ding, Y. Ye, et al., Food Chem 194 (2016) 1224–1229.
[12] Y.W.L. Liu, W. Fu, Sens. Actuators B: Chem. 247 (2017) 414–420.
[13] H. So, J. Byeong, C. Kim, Inorg. Chim. Acta 492 (2019) 83–90.
[14] M. Feng, Q. Zhang, X. Chen, et al., Biosens. Bioelectron. 210 (2022) 114294.
[15] H. Wei, E. Wang, Chem. Soc. Rev. 42 (2013) 6060.
[16] J. Hao, C. Zhang, C. Feng, et al., Chin. Chem. Lett. 34 (2023) 107650.
[17] X. Hai, Y. Li, K. Yu, et al., Chin. Chem. Lett. 32 (2021) 1215–1219.
[18] W. Liu, L. Chu, C. Zhang, et al., Chem. Eng. J. 415 (2021) 128876.
[19] P. Ren, Q. Li, T. Song, Y. Yang, ACS Appl. Mater. Interfaces 12 (2020) 27210–27218.
[20] G. Gan, X. Li, L. Wang, et al., ACS Nano 14 (2020) 9929–9937.
[21] N. Cheng, J.C. Li, D. Liu, Y. Lin, D. Du, Small 15 (2019) 1901485.
[22] X. Chen, M. Feng, X. Xie, et al., Talanta 246 (2022) 123487.
[23] X. Huang, J.T. Groves, Chem. Rev. 118 (2017) 2491–2553.
[24] Y. Shang, X. Duan, S. Wang, et al., Chin. Chem. Lett. 33 (2022) 663–673.
[25] B. Xu, W. Wang, L. Gao, et al., Angew. Chem. Int. Ed. 58 (2019) 4911–4916.
[26] L. Jiao, J. Wu, H. Zhong, et al., ACS Catal. 10 (2020) 6422–6429.
[27] J. Xia, Y. Shen, H. Zhang, et al., Ind. Crop. Prod. 187 (2022) 115449.
[28] Y. Zhu, R. Zhu, Y. Xi, et al., Appl. Catal. B: Environ. 255 (2019) 117739.
[29] C. Lai, X. Shi, L. Li, et al., Sci. Total. Environ. 775 (2021) 145850.
[30] X. Wang, J. Sun, T. Li, et al., Energy Storage Mater 36 (2021) 409–416.
[31] X. Wang, D. Wu, C. Dai, et al., J. Mater. Chem. A 8 (2020) 5105–5114.
[32] Z. Wu, C. Hou, Y. Qian, J. Chem. Eng. Data. 55 (2010) 3958–3961.
[33] Y. Shang, X. Xu, B. Gao, et al., Chem. Soc. Rev. 50 (2021) 5281–5322.
[34] H. Li, Q. Li, Q. Shi, et al., Food Chem 389 (2022) 132985.
[35] Y. Mao, S. Gao, L. Yao, et al., J. Hazard. Mater. 408 (2021) 124898.
[36] Q. Chen, S. Li, Y. Liu, et al., Sens. Actuators B: Chem. 305 (2020) 127511.
[37] H. Zhang, S. Hwang, M. Wang, et al., J. Am. Chem. Soc. 139 (2017) 14143–14149.
[38] A. Guan, Z. Chen, Y. Quan, et al., ACS Energy. Lett. 5 (2020) 1044–1053.
[39] X. Zhuang, L. Mao, Y. Li, Electrochem. Commun. 83 (2017) 96–101.
[40] X. Han, L. Liu, H. Gong, et al., Food Chem. 371 (2022) 131115.
[41] P. Chen, T. Zhou, L. Xing, et al., Angew Chem. Int. Ed. 56 (2017) 610–614.
[42] X. Wei, S. Wei, S. Cao, et al., Appl. Surf. Sci. 564 (2021) 150423.
[43] W. Fan, Z. Li, C. You, et al., Nano Energy 37 (2017) 187–194.
[44] L. Yang, J. Mi, J. Liang, et al., ACS Appl. Energy Mater. 2 (2019) 6295–6301.
[45] J. Li, J. Chen, H. Wan, et al., Appl. Catal. B: Environ. 242 (2019) 209–217.
[46] Y. Xu, J. Xue, Q. Zhou, et al., Angew. Chem. Int. Ed. 59 (2020) 14498–14503.
[47] L. Feng, L. Zhang, S. Chu, et al., Appl. Surf. Sci. 583 (2022) 152496.
[48] L. Chen, K. Xing, Q. Shentu, et al., Chemosphere 280 (2021) 130911.
[49] S. Singh, K. Mitra, A. Shukla, et al., Anal. Chem. 89 (2016) 783–791.
[50] H.H. Zeng, K. Yu, J. Huang, et al., Colloids Surf. B 204 (2021) 111796.
[51] Y. Gao, T. Li, Z. Chen, et al., Environ. Sci. Technol. 55 (2021) 8318–8328.
[52] X. Peng, J. Wu, Z. Zhao, et al., Chem. Eng. J. 427 (2022) 130803.
[53] Q. Chen, Y. Liu, Y. Lu, et al., J. Hazard. Mater. 422 (2022) 126929.
[54] B. Zhang, X. Li, K. Akiyama, et al., Environ. Sci. Technol. 56 (2021) 1321–1330.
[55] X. Wang, X. Pu, Y. Yuan, et al., Chin. Chem. Lett. 31 (2020) 2634–2640.
[56] B. Huang, Z. Wu, H. Zhou, et al., J. Hazard. Mater. 412 (2021) 125253.
[57] Y. Shang, X. Liu, Y. Li, et al., Chem. Eng. J. 446 (2022) 137120.
[58] J. Yang, P. Li, X. Duan, et al., J. Hazard. Mater. 430 (2022) 128463.
[59] J. Li, M. Li, H. Sun, et al., ACS Catal. 10 (2020) 3516–3525.
[60] E.T. Yun, J.H. Lee, J. Kim, et al., Environ. Sci. Technol. 52 (2018) 7032–7042.